



N.F. ASSOCIATES

N.S.

2005



138
844
THS

67964791

**LIBRARY
Michigan State
University**

This is to certify that the
thesis entitled

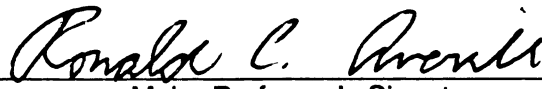
**MODELING AND DESIGN OPTIMIZATION OF GOLF
SHAFTS**

presented by

NICHOLAS FRANK ABBRUZZESE

has been accepted towards fulfillment
of the requirements for the

 M.S. degree in Mechanical Engineering



Major Professor's Signature

 7/25/05

Date

PLACE IN RETURN BOX to remove this checkout from your record.
TO AVOID FINES return on or before date due.
MAY BE RECALLED with earlier due date if requested.

DATE DUE	DATE DUE	DATE DUE
NOV 0 3 2003		
NOV 0 4 2003		

**MODELING AND DESIGN OPTIMIZATION OF
GOLF SHAFTS**

By

Nicholas Frank Abbruzzese

A THESIS

**Submitted to
Michigan State University
in partial fulfillment of the requirements
for the degree of**

MASTER OF SCIENCE

Department of Mechanical Engineering

2005

ABSTRACT

MODELING AND DESIGN OPTIMIZATION OF GOLF SHAFTS

By

Nicholas Frank Abbruzzese

There are a number of tests and methods used in the golf industry that attempt to measure and characterize golf shaft performance. The first portion of this work shows that these tests can be modeled and studied analytically using beam finite elements. In the second portion, the golf shaft is dynamically modeled and optimized within a finite element simulation of a golf swing. During the optimization, parameters of the golf shaft are varied and the performance is measured by the launch and spin characteristics of the golf ball after impact.

To my parents, John and Terry

ACKNOWLEDGEMENTS

I'd like to thank Dr. Tom Mase and Dr. Ron Averill for their support and guidance throughout this endeavor. I'd like to thank Dr. Mase for his patience and understanding. His willingness and devotion to seeing me through to the end, has never wavered. I'd like to thank Dr. Averill for his patience and unselfishness. He agreed to take this on at much later stage in my graduate program for which I am grateful. He also provided me with the motivation I needed at times of panic and doubt.

Most importantly, working with these two individuals has allowed me to grow in so many ways both personally and professionally.

TABLE OF CONTENTS

LIST OF TABLES	VII
LIST OF FIGURES	VIII
1 INTRODUCTION AND LITERATURE REVIEW	1
1.1 INTRODUCTION	1
1.2 LITERATURE REVIEW	2
2 SHAFT MODELING	6
2.1 OVERVIEW	6
2.1.1 <i>Beam Theories: Classical Euler-Bernoulli and Timoshenko</i>	6
2.1.2 <i>Shaft EI Measurement</i>	8
2.1.3 <i>Assumptions of Shaft Mass</i>	10
2.2 CALCULATION OF GOLF SHAFT ZONAL FREQUENCIES.....	12
2.2.1 <i>Background</i>	12
2.2.2 <i>The Finite Element Model</i>	13
2.2.3 <i>Numerical Results and Discussion</i>	17
2.3 MODELING OF KICKPOINT	21
2.3.1 <i>Background</i>	21
2.3.2 <i>Buckling ~ Finite Element Model</i>	22
2.3.3 <i>Buckling ~ Numerical Results and Discussion</i>	25
2.3.4 <i>Static Test ~ Finite Element Model</i>	26
2.3.5 <i>Static Test ~ Numerical Results and Discussion</i>	27
2.4 SUMMARY OF SHAFT MODELING	29
3 OPTIMIZATION USING COMMERCIAL CODES	30
3.1 OVERVIEW	30
3.2 THE “SILICON BYRON” MODEL	32
3.2.1 <i>The Shaft</i>	32
3.2.2 <i>The Club head</i>	34
3.2.3 <i>The “Arms”, “Wrists”, and “Hands”</i>	34

3.2.4	<i>The Swing: Loading, Joint Definitions, Contact Definitions</i>	35
3.2.5	<i>The ball</i>	37
3.3	HEEDS OPTIMIZATION OF SHAFT STIFFNESS	38
3.3.1	<i>Background / Aim</i>	38
3.3.2	<i>Baseline Design</i>	38
3.3.3	<i>Preparations for Optimization</i>	43
3.3.4	<i>Optimization Problem Definition</i>	45
3.3.5	<i>Model Variables, Responses, and Constraints</i>	47
3.3.6	<i>Results and Evaluation of Optimal Designs</i>	55
4	CONCLUSIONS AND DISCUSSION	59
4.1	SHAFT MODELING	59
4.2	OPTIMIZATION	59
4.3	FUTURE WORK	60
	BIBLIOGRAPHY	61

LIST OF TABLES

TABLE 1. GRAPHITE DRIVER BALANCE POINTS FOR DIFFERING MASS SHAFTS.....	10
TABLE 2. MASS PER UNIT LENGTH OF THE 12 SHAFTS MODELED.	11
TABLE 3. STANDARD NUMBER OF EI MEASUREMENTS MADE ALONG THE LENGTH OF A GOLF SHAFT.	16
TABLE 4. CRITICAL BUCKLING LOADS, LOCATIONS OF MAXIMUM DEFLECTION, AND LABELED STIFFNESS FOR EACH SHAFT (MEASURED FROM TIP).	26
TABLE 5. RESULTS OF STATIC TEST (MEASURED FROM TIP).	28
TABLE 6. ELEMENTS AND CORRESPONDING SECTIONS OF THE SHAFT.	33
TABLE 7. CLUB HEAD COMPONENTS.	34
TABLE 8. COORDINATES NEEDED TO DEFINE POLYNOMIALS WITH RANGES USED IN OPTIMIZATION. THE X COORDINATES RANGE OVER THE LENGTH OF SHAFT BEING OPTIMIZED (0-28.2 IN) WHILE THE Y COORDINATES RANGE OVER THE RADIUS AND THICKNESS VALUES RESPECTIVELY (ALL UNITS IN INCHES).	51
TABLE 9. CONSTRAINTS AND OBJECTIVE OF OPTIMIZATION.....	54
TABLE 10. BALL FLIGHT AND SPIN CHARACTERISTICS OF OPTIMAL DESIGNS.	58

LIST OF FIGURES

FIGURE 1. FIRST TRANSVERSE BENDING NATURAL FREQUENCY OF A SIMPLY-SUPPORTED BEAM AS A FUNCTION OF BEAM-LENGTH ASPECT RATIO (h/L) (FROM FRIEDMAN AND KOSMATKA [7]).....	7
FIGURE 2. DIAGRAM OF FLEX TEST APPLIED TO A SEGMENT OF GOLF SHAFT.	9
FIGURE 3. DEVICE FOR MEASURING EI PROFILE OF GOLF SHAFTS.	10
FIGURE 4. COMMON FREQUENCY MACHINE (FUJIKURA) USED FOR MEASURING ZONE FREQUENCIES.	12
FIGURE 5. BEAM ELEMENT DEGREES OF FREEDOM.	13
FIGURE 6. SUMMARY OF MODEL DETAILS AND BOUNDARY CONDITIONS.	18
FIGURE 7. RESULTS FROM THE ORIGINAL CLAMPED MODEL COMPARED WITH EXPERIMENTALLY MEASURED VALUES FOR THE 12 SHAFTS LISTED IN TABLE 2. THE ZONES CORRESPOND TO THE DIFFERENT CANTILEVERED LENGTHS WHILE THE BARS ARE THE FREQUENCY VALUES.	18
FIGURE 8. MEASURED CLAMP STIFFNESS OF FUJIKURA FREQUENCY MACHINE.	19
FIGURE 9. ZONAL FREQUENCIES CORRECTED BY ADDITION OF ROTATIONAL SPRING.....	20
FIGURE 10. COMPARISON OF FE MODEL SOLUTION WITH THAT FOUND BY EULER.	25
FIGURE 11. INITIAL STARTING POINT OF SWING SIMULATION.	39
FIGURE 12. SIMULATION AT 0.15 SECONDS.	39
FIGURE 13. SIMULATION AT 0.30 SECONDS.	40
FIGURE 14. SIMULATION AT 0.37 SECONDS.	40
FIGURE 15. SIMULATION AT 0.41 SECONDS.	41
FIGURE 16. SIMULATION AT 0.42 SECONDS.	41
FIGURE 17. SIMULATION JUST AFTER IMPACT AT 0.43 SECONDS.....	42
FIGURE 18. SIMULATION AT 0.44 SECONDS.	42
FIGURE 19. STIFFNESS PROFILE OF BASELINE SHAFT DESIGN.	43
FIGURE 20. SEQUENCE OF SWING SIMULATION.	45
FIGURE 21. VARIABLES INFLUENCING BACKSPIN.....	46

FIGURE 22. AN EXAMPLE POLYNOMIAL FOR THE OUTER RADIUS OF THE SHAFT. THE MAXIMUM AND MINIMUM ALLOWABLE RADIUS IS ALSO SHOWN.	49
FIGURE 23. AN EXAMPLE POLYNOMIAL FOR THE THICKNESS OF THE SHAFT. THE MAXIMUM AND MINIMUM ALLOWABLE THICKNESS IS ALSO SHOWN.	50
FIGURE 24. SEQUENCE OF ONE EVALUATION IN OPTIMIZATION.	53
FIGURE 25. OPTIMAL DESIGNS – GROUP 1. THE PROFILE IS THAT OF THE 28.2 INCH SPAN VARIED IN THE OPTIMIZATION.	56
FIGURE 26. OPTIMAL DESIGNS – GROUP 2. THE PROFILE IS THAT OF THE 28.2 INCH SPAN VARIED IN OPTIMIZATION.	57
FIGURE 27. DESIGN 65 EXHIBITING A HIGH DEGREE OF DEFORMATION IN DOWNSWING.	58

1 Introduction and Literature Review

1.1 Introduction

In recent years, the golf industry has been searching for more objective and technical means of characterizing golf shaft performance. Conventional terms and methods used in the industry have been shown to not accurately describe shaft performance; they remain too subjective and the methods by which they're determined lack consistency throughout the industry [1]. As a result, attempts are being made to better quantify and "fit" the performance of a certain shaft to a specific golfer's swing.

Currently there are two basic attributes used in evaluating golf shaft performance. These two attributes are also the cornerstones on which the shafts are marketed and sold. They consist of measures of the shaft's flex, or "stiffness," and "kickpoint". There are a wide range of experimental tests and methods used to measure these characteristics. What Chapter 2 will show is that a majority of these experimental tests can be accurately modeled using elementary beam finite element models. This is accomplished through an initial knowledge of the shaft's "bending profile" or "EI curve". The "bending profile" or "EI curve" is becoming a standard in the industry for benchmarking shaft designs [2]. Prior knowledge of this bending profile is what the elementary beam models rely upon. This will be discussed in further detail in Chapter 2.

Stemming from the bending profile and its increasing importance to the overall evaluation and design of golf shafts, an optimization study is also undertaken to find the optimal bending profile for a given golf swing. Certain design variables of the golf shaft are dynamically studied and optimized using a full-swing finite element simulation in LS-

DYNA. Unlike the static analyses of Chapter 2, the complete dynamic response of the shaft is evaluated and optimized. The details of the finite element model and of the optimization are presented in Chapter 3. The following section will provide a broad technical review of golf shafts.

1.2 Literature Review

Perhaps the best paper to lead this review is by G.P Horwood, “Golf Shafts – a technical perspective” [3]. Horwood acknowledges the impact of the golf shaft on the overall golf swings performance, while also acknowledging the extreme difficulty with finding consistent and technically sound ways of characterizing this performance. He warns of the sometimes extreme marketing hype that is used in the industry which leads golfers into believing that there are certain shafts fitted “perfectly” for their individual swings. He explains on a very simple level, that the characteristics of a golf shaft that are of most importance are the golf shaft’s bending and torsional stiffness. In the golf swing the inertia of the club head coupled with the offset of the club head center of gravity are what influence the golf shaft dynamics in the golf swing.

In the paper by Chou and Roberts the accuracy of three popular methods for the measurement of a golf shafts “kickpoint” are analyzed [1]. In their study three steel and three graphite golf shafts with a wide range of kickpoints were chosen. The six drivers were then subjected to machine testing. The goal was to relate the changes in ball trajectory to the variations in shaft kickpoint. Classical golf theory has always suggested that the degree and location of a golf shafts kickpoint has a direct influence on ball trajectory. However, the conclusions made by Chou and Roberts showed a poor correlation.

Wallace and Hubbell examined the influence of golf shaft stiffness on the swing kinematics and dynamics of a group of amateur golfers [4]. Each golfer was asked to hit 3-10 shots with each of 3 different 5-irons varying only in shaft stiffness. Variables considered in the study included club head speed, handicap, ball speed, clubface angle, swing-path angle, as well as a few others. Although this study provided and reaffirmed some of the general conclusions made about the differences between low and high handicappers, it failed in drawing any sound conclusions in regards to shaft stiffness. This was due to analyzing the golfers as a group, rather than looking at how shaft stiffness might affect an individual golfer. Wallace and Hubbell also acknowledged that the study did not take into account important launch conditions like ball launch angle and spin rate.

The work by Butler and Winfield attempts to find a better understanding of shaft dynamics in the downswing along with finding key variables that affect the dynamic performance [5]. Their study consisted of a finite element model along with certain experimental measurements of shaft deflection and twisting during the downswing. The finite element beam model developed by Butler and Winfield helped to show the influence of the club head's offset center of gravity to the twisting of the shaft. The first mode of the shaft was analyzed and a simple correlation was made between the deflection of the shaft and the coupled twisting of the club head. The most significant portion of the paper was the experimental measurements that provided some very basic insight into the shaft deflection in the downswing. Measurements of the "lead/lag" deflection which occurs in the actual plane of the golf swing and measurements of the "toe up/down" deflection occurring in the out of plane direction were made for 3 varying swing types.

The conclusions certainly helped in finding a better understanding of the dynamics of the golf shaft. Butler and Winfield also acknowledged the importance and possible use of such measurements for club-fitting.

Brouillette details three non-destructive methods of measuring the flexural rigidity distribution along the length of a golf shaft [6]. These are alternative and out-dated methods for measuring the EI profile referred to in Chapter 2. The methods discussed by Brouillette are sound and may have influenced the current method used in the industry today.

Mase documents a new method, which is quickly becoming industry standard, for measuring the EI profile of golf shafts [2]. The paper details a method for correction of the radial deflections when measuring the bending stiffness profile or EI profile of golf shafts (see Sec. 2.1.2).

The work by Friedman and Kosmatka is mentioned here to support the elementary beam modeling in Chapter 2 [7]. The models were developed using simple Euler-Bernoulli beam finite elements. Initially the frequencies of the shorter beam models, those having a somewhat larger aspect ratio, were found to be too stiff. It was originally thought that due to the beams shorter length that the shear effects could not be neglected. This led to the investigation of Timoshenko beam finite elements. Figure 1 in Chapter 2 is referenced from the study. This figure proves that even the shortest shaft lengths examined in the study can be accurately modeled by Euler-Bernoulli finite elements.

The work by Lee and Kim is one of the very few optimization studies directly applied to golf equipment [8]. In it they detail an optimization method for graphite golf shafts. The objective function is to minimize the torque of the shaft, while satisfying

certain constraints like flex, “kick point”, and weight requirements. This is accomplished using a finite element model developed in ABAQUS interfaced with genetic algorithm type optimization software specifically for composite materials called DARWIN.

2 Shaft Modeling

2.1 Overview

There are a number of technical tests and methods used in the golf industry that attempt to measure golf shaft performance. Bending stiffness, torsional stiffness, kickpoint, durability, and conformity to the Rules of Golf are major factors in shaft design and manufacture. In this thesis, two main areas of shaft performance were considered: a measure of the shaft's overall stiffness behavior, and a measure of the shafts "kickpoint" or "flexpoint" behavior.

What this chapter will show is that the majority of these tests, which in some cases involve rather intensive and elaborate experimental setups, can be accurately modeled analytically by using beam finite elements. Conclusions drawn from these models can also be used to validate or reject their relevance in describing shaft behavior. And in some cases the models can even eliminate the need for experimental testing, thereby reducing the time and cost of such testing.

The following sections provide an introduction to the models. Basic beam theory is reviewed and important assumptions and key points in the modeling are discussed. The models were implemented using the MATLAB program version 7.0.0.19920 (R14).

2.1.1 Beam Theories: Classical Euler-Bernoulli and Timoshenko

The Euler-Bernoulli and Timoshenko beam theories are two of the most commonly used beam theories in structural mechanics problems. However the underlying assumptions found in the two theories are slightly different.

In the Euler-Bernoulli theory shear effects are neglected and as a direct result the cross-section of the deformed beam must remain plane and normal to the longitudinal axis. On the other hand, the Timoshenko theory includes shear effects, therefore allowing the cross-section to remain plane but not necessarily normal to the deformed axis. For slender beams, those defined as having a beam-thickness-to-length aspect ratio much less than one-tenth ($h/L < 0.1$), the Euler-Bernoulli beam theory tends to give good approximations because transverse shear deformation is negligible. However, as the beam becomes thick and non-slender ($0.1 < h/L < 1.0$) transverse shear deformation must be included and the Timoshenko model should be considered [7]. The figure below is borrowed from Reference [7] and summarizes their conclusions.

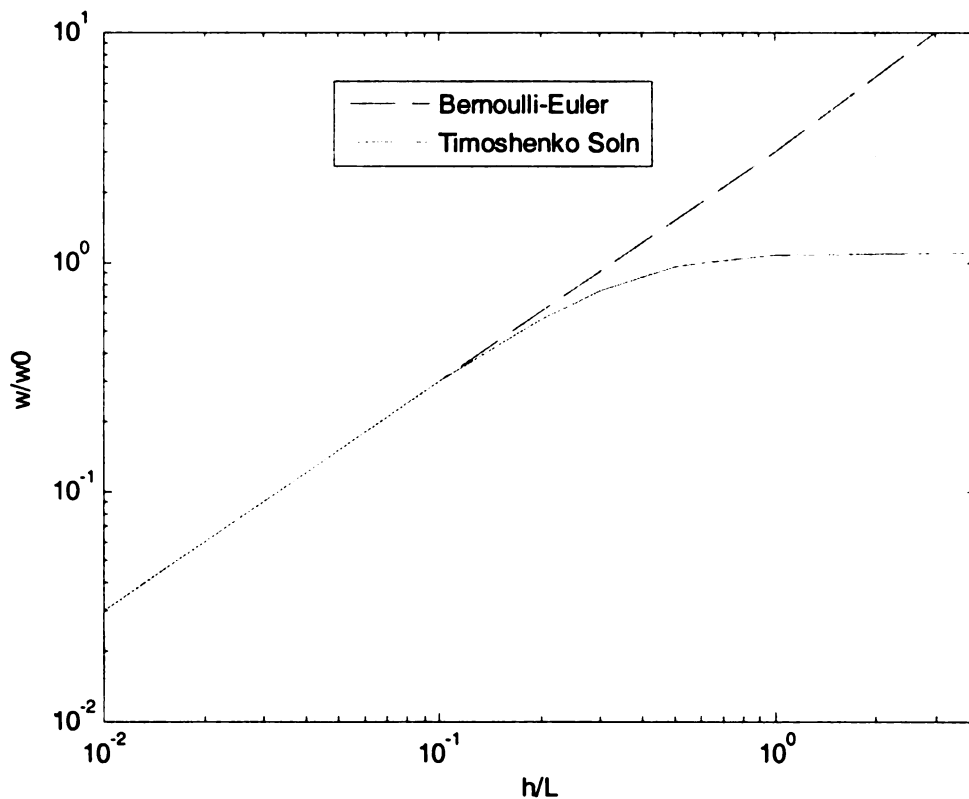


Figure 1. First transverse bending natural frequency of a simply-supported beam as a function of beam-length aspect ratio (h/L) (From Friedman and Kosmatka [7])

At the outset of the study there was doubt as to which theory was most appropriate for modeling the shorter golf shaft lengths. The initial results from the models of the shorter shaft lengths were overly stiff and it was thought that the Timoshenko theory would provide better results. However, according to the figure above, it was concluded that the traditional Euler-Bernoulli theory should be sufficient and accurate. The overly stiff predictions were later attributed to the boundary conditions, as discussed in the sequel.

When considering the cantilevered golf shafts in this study, the shortest length is 15 inches while the shaft diameter is approximately 0.5 inches. This gives a beam-thickness-to-length aspect ratio no larger than 0.03. Therefore, the Euler-Bernoulli beam theory is assumed appropriate and is used in the development of all finite element models.

For a more detailed look at the finite element formulations of both the classical Euler-Bernoulli theory and the Timoshenko theory, see Reddy [9].

2.1.2 Shaft EI Measurement

A fairly technical approach to help characterize shaft performance is to measure the shaft's "bending profile" or " EI curve" (E = modulus of elasticity, I = moment of inertia or second moment of area). As will be seen, this EI curve is the key to the development of all finite element models in this part of the study. The data found from these measurements are direct inputs to the finite element models. A brief description of the method used in obtaining these measurements is now discussed.

The modulus of elasticity is a measure of material stiffness and moment of inertia is a measure of material distribution. Together, they make up a structural stiffness per

unit length. True stiffness, EI/L , is not used since a constant span length of 250 mm is used in the experimental apparatus. The profile consists of a series of bending measurements taken along the length of the shaft. From end to end, incremental spans of the shaft are subjected to what is called a three point flex test; two ends are simply supported while a point load is applied at the mid-span. Under this type of loading, a simple mechanics of materials relation can be used to provide a local estimation of the shaft's bending stiffness or EI .

$$EI = \frac{PL^2}{48\delta_c} \quad (2.1-1)$$

Here P is the applied load, L is the span length, and δ_c the beam deflection at the mid-span. Figure 2 is an example showing a schematic of the flex test. The actual test machine for measuring shafts is shown in Figure 3.

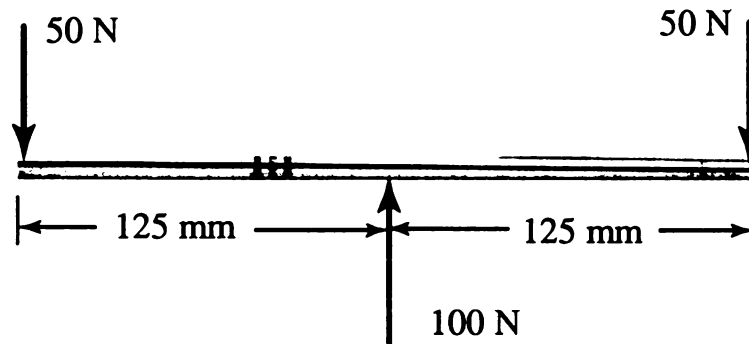


Figure 2. Diagram of flex test applied to a segment of golf shaft.

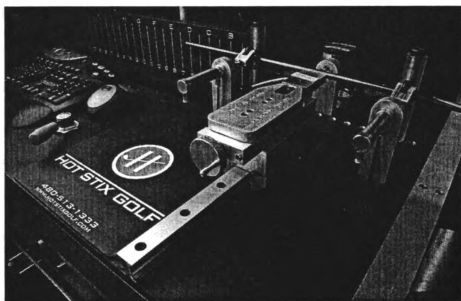


Figure 3. Device for measuring EI profile of golf shafts.

These bending profiles provide insight into how the shaft's bending stiffness changes along its length. This information becomes the foundation for modeling the golf shaft.

2.1.3 Assumptions of Shaft Mass

Another key assumption made in the modeling is in regards to the golf shaft mass.

The mass is assumed to be distributed evenly along the length of the shaft. Table 1 shows the relationship between the shaft mass and its distribution about its balancing point. These shafts were selected in order to include the range of weights and designs currently available. The numbers reported are an average of n different shafts that were measured.

Table 1. Graphite driver balance points for differing mass shafts.

Shaft	Mass, g	Balance Point %
Graphite Shaft 1 (n=4)	54.75	51.9
Graphite Shaft 2 (n=4)	65.5	52.2
Graphite Shaft (n=3)	70.3	51.4
Graphite Shaft (n=3)	82	53.1

The mass of both steel and graphite shafts are distributed quite evenly about the balance point. Further support for this assumption stems from the inverse relationship between a typical shaft diameter and its thickness.

In the subsequent finite element models, the mass per unit length ρ_L is calculated as an average for each shaft and is found by dividing the recorded shaft mass by the overall length. Table 2 shows the 12 shafts used in the models and their assumed mass per unit length.

Table 2. Mass per unit length of the 12 shafts modeled.

Model	Flex	Length (in)	Weight (g)	Mass per unit Length (kg/m)
YS-6	R	46	63	0.0539
YS-6	S	46	64	0.0548
YS-6	SX	46	65	0.0556
YS-6	X	46	65	0.0556
YS-6	TX	46	68	0.0582
YS-7	R	46	76	0.0650
YS-7	S	46	77	0.0659
YS-7	SX	46	78	0.0668
YS-7	X	46	78	0.0668
YS-7	TX	46	79	0.0676
YS-8.1	S	46	86	0.0736
YS-8.1	SX	46	87	0.0745

2.2 Calculation of Golf Shaft Zonal Frequencies

2.2.1 Background

The shaft's first natural frequency at various cantilevered lengths are measured and are referred to as "zonal frequencies" in industry. The frequencies at cantilevered lengths of 991, 787, 584, and 381 mm (39, 31, 23, and 15 inches respectively) are determined experimentally using a modified Fujikura frequency machine (Figure 4). These "zonal frequencies" are being used as yet another way to characterize shaft stiffness and performance.

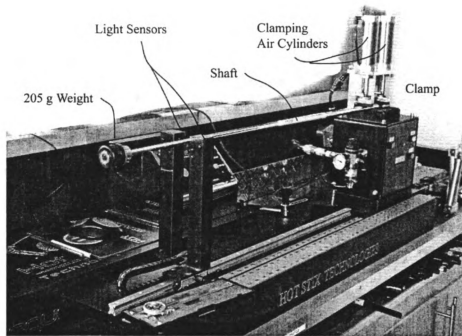


Figure 4. Common frequency machine (Fujikura) used for measuring zone frequencies.

Currently, as the popularity of these new methods increases and as new shaft designs are constantly emerging, large databases must be kept to include the measured data. The following will show that a simple beam finite element model can accurately predict the zonal frequencies from the measured bending profile. Therefore reducing the

time and cost associated with experimentally measuring the zonal frequencies. The finite element formulation and complete description of the model will be highlighted followed by a comparison of numerical results for 12 shafts.

2.2.2 The Finite Element Model

The golf shaft is modeled as a cantilever beam with a point mass included at the tip to represent the club head. Like most cantilever beams, the original model was clamped at one end having both the transverse and rotational displacement of one node constrained. However, as it will be explained in the results, this original model had to be modified. The constrained end of the shaft was remodeled to include a simple support along with a stiff rotational spring. The simple support continued to constrain the transverse displacement, but the rotational spring was needed to model a small amount of compliance in the rotation of the joint.

The discretization of the beam is accomplished using a number of Euler-Bernoulli finite elements. Use of simple Euler-Bernoulli beam elements was justified in Section 2.1.1. A typical depiction of the element can be seen in Figure 5. Each element has two nodes each with two degrees of freedom; a transverse displacement w , and a cross-section rotation θ .

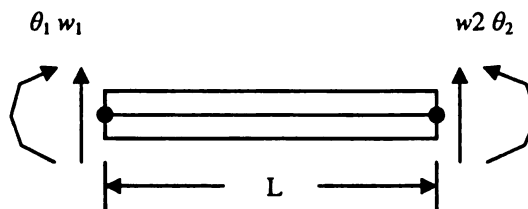


Figure 5. Beam element degrees of freedom.

The formulation of the stiffness matrix and the mass matrix for a single element can be found in many introductory finite element textbooks [9,10]. It will be briefly summarized here for the sake of completeness.

The strong form of the Euler-Bernoulli free vibration equation is given as

$$\rho_L \frac{\partial^2 w}{\partial t^2} + \frac{\partial^2}{\partial x^2} \left(EI \frac{\partial^2 w}{\partial x^2} \right) = 0 \quad (2.2-1)$$

where ρ_L is the mass per unit length, EI the bending stiffness, and $w(x,t)$ the transverse displacement of the beam. The strong form here requires the solution of $w(x,t)$ to be of the C4 type having continuous 4th order derivatives. The weak form, as it will be shown, will allow this restriction to be “weakened” to require a solution of C2 type, which requires only continuous 2nd order derivatives.

To arrive at the weak form of the equation, Equation 2.2-1 is multiplied by an arbitrary test function $\bar{w}(x,t)$ and integrated over the domain. Provided that the test function is zero wherever an essential boundary condition exists; the final result simplifies to

$$\int_0^L \rho_L \frac{\partial^2 w}{\partial t^2} \bar{w} dx + \int_0^L EI \frac{\partial^2 w}{\partial x^2} \frac{\partial^2 \bar{w}}{\partial x^2} dx = 0 \quad (2.2-2)$$

where the domain is considered over the entire length of the member.

The next step is to then discretize the weak form of the equation. The displacement across each element is assumed to take on the form

$$w(x,t) = N_1(x)w_1(t) + N_2(x)\theta_1(t) + N_3(x)w_2(t) + N_4(x)\theta_2(t) \quad (2.2-3)$$

where $N_1, N_2, N_3,$ and N_4 are Hermitian cubic interpolation functions (also called shape functions). These are time independent and are used to ensure continuity across the elements.

Using the discretization above in the weak form yields the finite element mass and stiffness matrices. The entries are given by the following

$$M_{\alpha\beta} = \int_0^L \rho_L N_\alpha(s) N_\beta(s) ds \quad \alpha, \beta = 1, 2, 3, 4 \quad (2.2-4)$$

$$K_{M\alpha\beta} = \int_0^L EI \frac{\partial^2 N_\alpha(s)}{\partial s^2} \frac{\partial^2 N_\beta(s)}{\partial s^2} ds \quad \alpha, \beta = 1, 2, 3, 4 \quad (2.2-5)$$

where a local coordinate system “s” has been introduced for ease in computing the relative entries.

The resulting consistent mass and material stiffness matrices for a single Euler-Bernoulli finite element are

$$\mathbf{K}_M = \frac{EI}{L^3} \begin{bmatrix} 12 & 6L & -12 & 6L \\ & 4L^2 & -6L & 2L^2 \\ & & 12 & -6L \\ \text{symmetric} & & & 4L^2 \end{bmatrix} \quad (2.2-6)$$

and

$$\mathbf{M} = \frac{\rho_L L}{420} \begin{bmatrix} 156 & 22L & 54 & -13L \\ & 4L^2 & 13L & -3L^2 \\ & & 156 & -22L \\ \text{symmetric} & & & 4L^2 \end{bmatrix} \quad (2.2-7)$$

where L is the element length, and the mass per unit length ρ_L and bending stiffness EI are assumed constant over the element.

As seen in the matrices above, approximations in the model are needed for each element’s bending stiffness EI , and mass per unit length ρ_L . The latter of the two is

approximated by dividing the total mass of the shaft by its length, giving an average value of ρ_L for all elements. This is a fair approximation because the mass along the length of the shaft can be considered relatively constant (see Sec. 2.1.3).

The approximation for each element's bending stiffness comes from prior knowledge of the shafts bending profile (see Sec. 2.1.2, [2]). This measured bending profile or *EI* curve provides approximate values of the shaft's bending stiffness along its length. The shaft is flexed over a 250 mm (10 in) span and a load ranging from 67 to 100 Newtons (15-23 lbs) is applied to the mid-span. This procedure is repeated every 50 mm (2 in) along the shaft up to 975 mm (39 in). The location of the point load is taken as the point at which the bending stiffness is evaluated. The table below details the location of each measurement taken along the shaft.

Table 3. Standard number of *EI* measurements made along the length of a golf shaft.

EI Measurement Number	Location of Measurement from Tip End (mm)	Applied Region of Shaft in Models (mm)
1	125	0 - 150
2	175	150 - 200
3	225	200 - 250
4	275	250 - 300
5	325	300 - 350
6	375	350 - 400
7	425	400 - 450
8	475	450 - 500
9	525	500 - 550
10	575	550 - 600
11	625	600 - 650
12	675	650 - 700
13	725	700 - 750
14	775	750 - 800
15	825	800 - 850
16	875	850 - 900
17	925	900 - 950
18	975	950 - 1000

Also shown in Table 3 are the regions of shaft in the model over which each measurement is assumed to apply and be constant. For example, the first measurement taken near the tip of the shaft at 125 mm is applied to the first 150 mm of the shaft in the model. These regions helped determine where elements should be divided and placed. As it turned out, dividing each region into two elements was sufficient enough for the frequencies to converge. All elements, except for those at the very ends of the model, are 25 mm in length.

Various cases were studied to test the validity of the models meshing as well as the logic used in assigning the EI measurements to regions. The original mesh was refined to contain twice the number of elements and there was a negligible change in the frequencies. In another case, the EI measurements were fit with a 4th-degree polynomial aiming to smooth the transition of the EI values between elements. This was also shown to have a negligible change in the resulting frequencies.

2.2.3 Numerical Results and Discussion

Given the bending profile data for 12 graphite-epoxy shafts, the zonal frequencies for each shaft could be computed using the finite element model presented. Results from the original clamped model and results from the model using the rotational spring are presented. Details of the various models are shown in Figure 6.

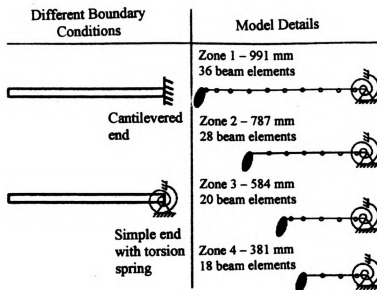


Figure 6. Summary of model details and boundary conditions.

The results from the original clamped model can be seen in Figure 7. The computed zonal frequencies are compared to the experimentally measured frequencies.

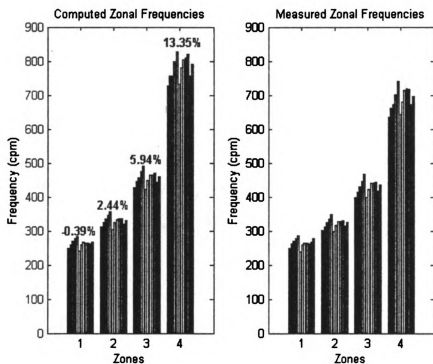


Figure 7. Results from the original clamped model compared with experimentally measured values for the 12 shafts listed in Table 2. The zones correspond to the different cantilevered lengths while the bars are the frequency values.

The computed frequencies become overly stiff as the shaft length shortens. The average error for the first zone is less than 1 percent, while the error for the second, third, and fourth zones increases to 2.44, 5.94, and 13.35 percent, respectively. This led to a closer inspection of the experimental equipment used to measure the frequencies.

The Fujikura machine was found to have a small amount of compliance in the clamped joint. The joint was in-effect, only semi-rigid. The air cylinders used for clamping the shaft make measurements easily and quickly attainable, but build in this small amount of compliance. Therefore, the original finite element model was modified to account for this small, rotational flexibility and a rotational spring was added to the end node. The stiffness of the clamp was measured and the following figure shows the linear fit of the stiffness value.

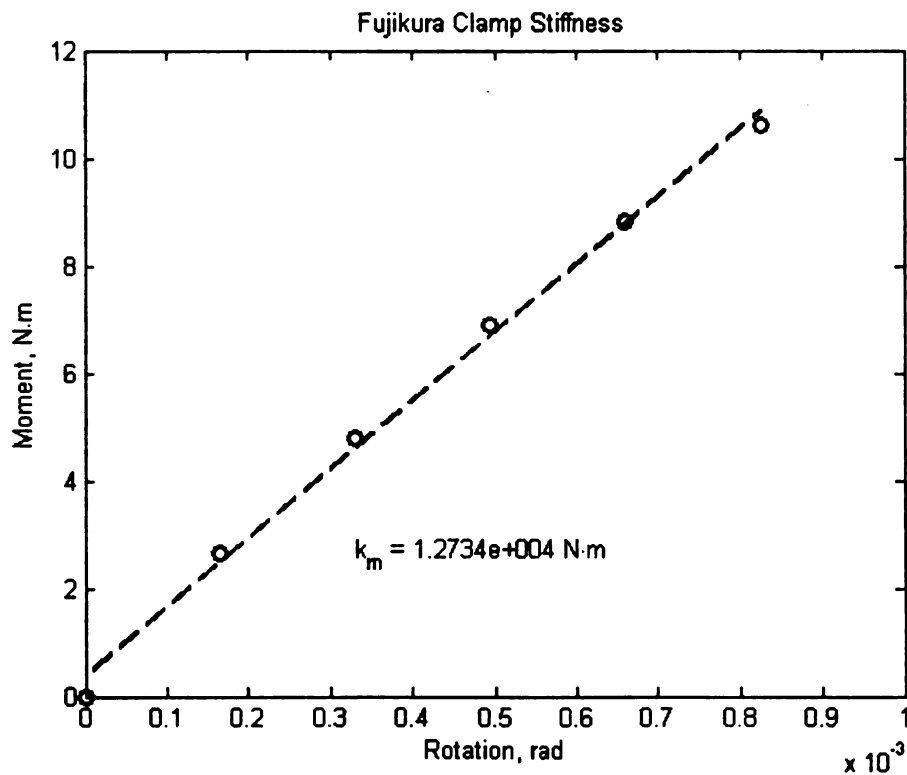


Figure 8. Measured clamp stiffness of Fujikura frequency machine.

Using the measured rotational stiffness in the finite element models greatly improved the error in the measurements of the shorter lengths without altering the accuracy of the longer lengths. Figure 9 shows the corrected frequency plots with the average error listed above each zone.

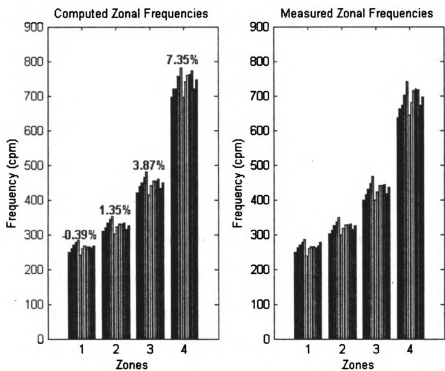


Figure 9. Zonal frequencies corrected by addition of rotational spring.

Although the error at the shorter shaft lengths does improve significantly, it still falls short of accurately predicting the frequencies for zones 3 and 4. Further modeling and investigation of the clamping mechanism is needed. Other sources of error contributing to this discrepancy could involve the experimental measurement device. The light sensor may have difficulty measuring the higher frequencies, therefore under-predicting the measured results.

2.3 Modeling of Kickpoint

2.3.1 Background

A golf shaft's "kickpoint", also referred to as "flex point" or "bend point", remains an issue of much debate in the golf industry. There are many terms, and just as many methods that are used in hopes of characterizing this aspect of golf shaft performance. The goal is to effectively relate the degree and location of a golf shaft's "flex" during the downswing to the resulting ball flight and trajectory. It is thought that a shaft with high "kickpoint" will result in lower ball flight, whereas a low "kickpoint" will result in higher ball flight.

One of the many proposed methods for determining a shaft's "kickpoint" is by analyzing its buckling behavior. This test consists of applying an increasing axial load to the shaft until buckling is reached. The evaluation of the shaft's "kickpoint" is then found from the buckled shape of the shaft. The maximum point of deflection and the corresponding location are then used to quantify and characterize the shaft "kickpoint".

Yet another method that will be modeled in the sections that follow consists of a simple static test. The shaft is clamped near the butt end and a specified load (usually of 2-lb or 8.9N) is hung from the tip of the shaft. A string is then connected between the two ends of the shaft creating a line of reference. The point at which the shaft is furthest from the string is noted and used as a relative evaluation of the "kickpoint". The static test remains controversial and has fallen short of being an accurate means of describing "kickpoint" as the finite element model will show.

2.3.2 Buckling ~ Finite Element Model

By definition, buckling is the bifurcation or branching of equilibrium states from stable to unstable. The analysis most commonly used in engineering practice with respect to buckling is what is known as linearized prebuckling analysis (LPB) [11,12]. In this analysis, solving a traditional linear algebraic eigenvalue problem involving the tangent stiffness matrix \mathbf{K}_t can assess the stability of a structure. The resulting eigenproblem yields the magnitude of the load at which buckling occurs (lowest eigenvalue) as well as the corresponding buckled shape of the column (corresponding eigenvector). The key steps and assumptions in LPB will be briefly summarized.

In LPB analyzing the tangent stiffness matrix \mathbf{K}_t assesses the stability of the structure. Here μ_i and z_i are the i^{th} eigenvalue and eigenvector, respectively, of the matrix.

$$\mathbf{K}_t z_i = \mu_i z_i \quad (2.3-1)$$

Since the tangent stiffness matrix is *real symmetric* all of its eigenvalues are therefore *real*. However as certain parameters are varied, in most cases the loading of the structure, the eigenvalues μ_i of the tangent stiffness matrix change and the matrix can become singular.

$$\mathbf{K}_t = \mathbf{K}_t(\lambda) \quad (2.3-2)$$

It is at this point, where the system transitions from a region of strong stability ($\mu_i > 0$) to neutral stability and singularity ($\mu_i \geq 0$) and into instability ($\mu_i < 0$). The point at which the matrix becomes singular is therefore considered to be the critical value denoted as λ_{cr} .

$$\det \mathbf{K}_t(\lambda_{cr}) = 0 \quad (2.3-3)$$

Loading the structure beyond this value initiates bifurcation and the structure will buckle.

The exact formulation of the buckling problem involves the decomposition of the tangent stiffness matrix \mathbf{K}_t into the material and geometric stiffness matrices \mathbf{K}_M and \mathbf{K}_G , respectively.

$$\mathbf{K} = \mathbf{K}_M + \mathbf{K}_G \quad (2.3-4)$$

The material stiffness \mathbf{K}_M is a function of the physical properties in the element and is constant, whereas the geometric stiffness \mathbf{K}_G is dependent upon the load in the element. As noted above the stability test requires that \mathbf{K}_t be singular, which leads to the final form of the stability eigenproblem.

$$\mathbf{K}_t z_i = (\mathbf{K}_M + \lambda_i \mathbf{K}_G) z_i = 0 \quad (2.3-5)$$

The critical loads required for buckling can now be obtained directly from the solution of the above equation. The eigenvalue λ_i closest to zero is the lowest critical load needed to reach buckling, while the corresponding eigenvector z_i is the buckling mode shape.

In the analytical model presented, each shaft is again discretized into a sufficient number of classical Euler-Bernoulli beam elements. The shaft length used in the model is 1.05m (41.5 in). The element material stiffness matrix was given previously in Equation 2.2-6 but is repeated here along with the exactly integrated geometric stiffness matrix [10,12].

$$\mathbf{K}_M = \frac{EI}{L^3} \begin{bmatrix} 12 & 6L & -12 & 6L \\ & 4L^2 & -6L & 2L^2 \\ & & 12 & -6L \\ \text{symmetric} & & & 4L^2 \end{bmatrix} \quad (2.3-6)$$

and

$$\mathbf{K}_G = \frac{P}{30L} \begin{bmatrix} 36 & 3L & -36 & 3L \\ & 4L^2 & -3L & -L^2 \\ & & 36 & -3L \\ \text{symmetric} & & & 4L^2 \end{bmatrix} \quad (2.3-7)$$

where P is the axial force in the element. In the simple case of modeling the golf shaft, the structure is statically determinate therefore allowing P to equal the applied load.

With the element matrices defined, the final steps involve assembling the global matrices and applying constraints to the model. The ends of the shaft are constrained by simple supports or pins eliminating their translational degrees of freedom.

The accuracy of the model was verified through comparison with the well known *Euler's method*, published in 1744. For a uniform beam/column of constant material and geometric properties subjected to an axial load, *Euler's Formula* gives the lowest critical buckling load.

$$F_{cr} = \frac{EI\pi^2}{L^2} \quad (2.3-8)$$

The beam used as a test case in the model had a bending stiffness of $EI = 50 \text{ Nm}$ and a length of 1.05m (41.5 in).

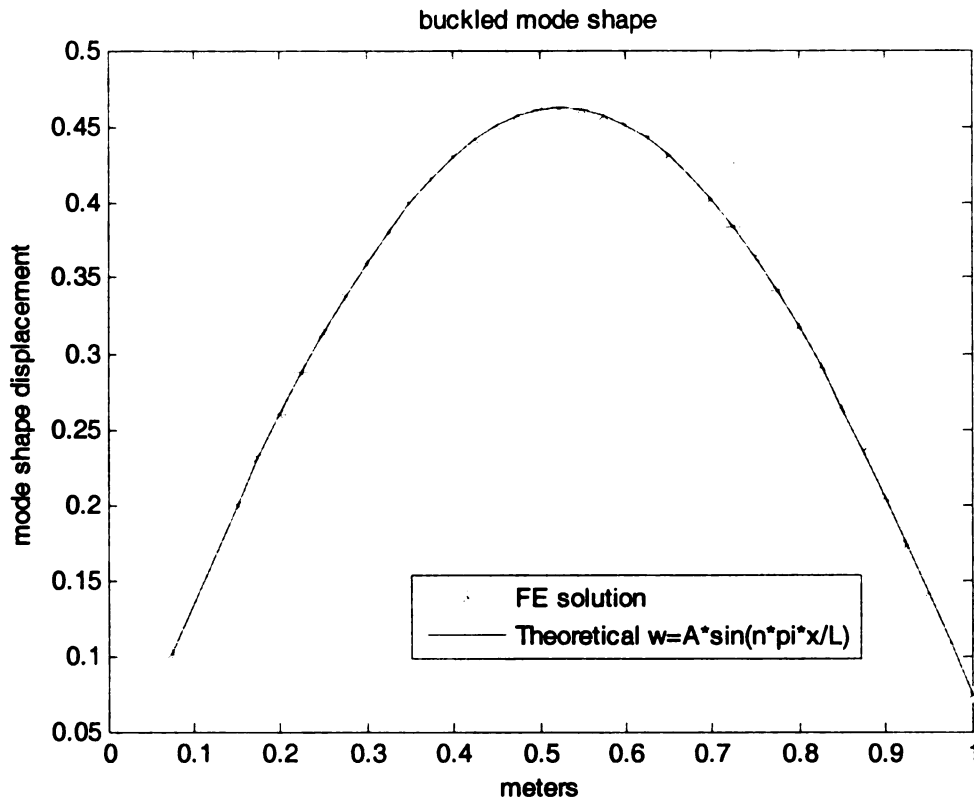


Figure 10. Comparison of FE model solution with that found by Euler.

Figure 10 shows the buckled mode shape compared with the theoretical solution obtained by Euler. The comparison of the critical loads is shown below where the superscript *E* represents the solution found using *Euler's Formula*.

$$F_{cr} = 444.126N \quad F_{cr}^E = 444.126N \quad (2.3-9)$$

The results from the finite element model are in complete agreement with the results found by using *Euler's Method*.

2.3.3 Buckling ~ Numerical Results and Discussion

Given the bending profile data for the group of 12 shafts, the critical buckling loads F_{cr} and the location of maximum deflection could be computed using the finite element model and LPB analysis presented.

Table 4 shows the calculated critical loads for each shaft, the location of maximum deflection from the tip end, as well as each shafts industry labeled stiffness. As seen, the magnitude of the critical load is directly related to the stiffness of the shaft but there is no discernable relation with the points of maximum deflection.

Table 4. Critical buckling loads, locations of maximum deflection, and labeled stiffness for each shaft (measured from tip).

Fcr (N)	Pt of Max. Deflection (m)	Stiffness Label
279.75	0.456	R
305.43	0.459	S
316.66	0.448	SX
343.11	0.453	X
365.18	0.456	TX
274.55	0.464	R
311.89	0.464	S
330.91	0.464	SX
332.57	0.465	X
339.69	0.468	TX
302.58	0.46	S
325.28	0.462	SX

The range of values shown for the locations of maximum deflection is very small, therefore making the characterization of the shafts “kickpoint” very difficult. This fact is well known to those in the golf industry.

2.3.4 Static Test ~ Finite Element Model

The static test for determining flex point can be modeled as a simple cantilever beam subjected to a tip load. The unknown displacements w are found from the solution to the equation below

$$\mathbf{K}w = \mathbf{F} \quad (2.3-10)$$

where \mathbf{K} is the global material stiffness matrix and \mathbf{F} the equivalent nodal force vector.

As in the other models, the shaft was discretized into a sufficient number of Euler-Bernoulli finite elements. The element material stiffness matrix \mathbf{K}_m was given previously in Equation 2.2-6, and the global matrix \mathbf{K} was assembled from each element stiffness matrix \mathbf{K}_m .

The only applied force in the model is the tip load of 0.907-kg (2-lb), which was modeled as an equivalent nodal force in the transverse direction. The equivalent nodal force vector therefore consists of only one non-zero entry corresponding to the node at the tip of the shaft.

The accuracy of this model could be verified through comparison to a well-known strength of materials solution. Given a uniform cantilever beam subject to a tip load, the exact solution for the maximum displacement is given by

$$w_{MAX} = -\frac{PL^3}{3EI} \quad (2.3-11)$$

where P is the applied load, L the length of the beam, E the young's modulus, and I the moment of inertia. The beam used to validate the model had a length of $L = 1.05\text{m}$, load of $P = 10.0\text{ N}$, and combined stiffness $EI = 50\text{ N}\cdot\text{m}^2$. The maximum displacement was calculated to be -0.0772 m and compares exactly with the result from the strength of materials solution.

2.3.5 Static Test ~ Numerical Results and Discussion

Given the bending profile data for the group of 12 shafts, the location of maximum deflection could be computed using the static finite element model presented. Table 5 summarizes the results.

Table 5. Results of Static Test (measured from tip).

Pt of Max. Deflection (m)	Stiffness Label
0.537	R
0.54	S
0.531	SX
0.536	X
0.539	TX
0.543	R
0.542	S
0.543	SX
0.544	X
0.547	TX
0.538	S
0.541	SX

As with the buckling results, the static test results are also inconclusive and lend little insight into characterizing or making any kind of distinction regarding “kickpoint”.

2.4 Summary of Shaft Modeling

It has been shown that many of the golf industry tests used to characterize golf shaft performance can be modeled and studied. With prior knowledge of the shaft's bending profile or EI curve, a number of these industry standard tests can be modeled.

The zonal frequencies test, which serves to characterize overall shaft stiffness, was first modeled. The calculation of the zonal frequencies matched well with the experimentally measured values at the lower shaft zones, with a slight over-prediction at the higher zones. Further investigation of the Fujikura frequency machine is recommended in order to pinpoint the cause of this error.

The purpose of the next two tests modeled was to help characterize shaft kickpoint. This term is rather loosely defined and its measurement has never been standardized across the industry. It was shown that modeling of these two tests is possible; however their inconclusive results proved that their relevance in describing this property of golf shafts is rather poor.

3 Optimization using Commercial Codes

3.1 Overview

In the previous Chapter it was shown that certain tests and methods used for measuring and quantifying golf shaft performance can be easily modeled and studied analytically. The characteristics of the shaft's stiffness and bending properties were studied without concern for the dynamics of the shaft in an actual golf swing. In the current Chapter a broader study is undertaken, in which the shaft is dynamically modeled and optimized using the full-simulation of a golf swing. During the optimization, parameters of the golf shaft are varied and the performance is measured by the launch and spin characteristics of the golf ball after impact.

Dr. Tom Mase of the *Composite Materials & Structures Center* at MSU provided the initial finite element model used in the study. It was originally created by Dr. Mase to model the mechanical swing machines used in the golf industry affectionately known as "Iron Byron". However it soon became apparent that the model could also be utilized in an optimization study of the golf shaft bending stiffness. The initial model was then modified accordingly.

The swing is simulated using LS-DYNA, which is a commercially available finite element software capable of nonlinear dynamic analyses. The club and golf swing are modeled as well as the golf ball and its impact with the club during the swing. LS-DYNA was chosen for this simulation because of its specific capabilities of modeling contact-impact interfaces. The software originated from a need for the stress analysis of structures subjected to various impact loadings. The overall model consisted of the ball,

the club head and shaft, and rigid connections used to represent the arms, wrists, and hands. Details of the model will be fully explained in the following sections.

The optimization of the golf shaft was accomplished through interfacing the LS-DYNA swing simulation with the commercial optimization software HEEDS (Hierarchical Evolutionary Engineering Design System). Parameters of the shaft stiffness were changed in each swing by HEEDS and each evaluation's performance was measured until optimal solutions were reached. Each run of the swing simulation was evaluated under certain constraints and objectives concerning the golf ball flight and spin. Further details and the results of the optimization will be discussed in later sections as well.

3.2 The “Silicon Byron” Model

3.2.1 The Shaft

The golf shaft was modeled in LS-DYNA using 3-node beam elements. The material was declared as linear elastic. There were a total of 37 beam elements, which made up 32 distinct sections (Table 6). Each section contained specific geometric properties that were used as variables in the optimization study. Details on the use of these sections and variables will be discussed in detail in the following section on optimization. The particular initial design for the shaft was taken as a long time popular steel stiff shaft (True Temper Dynamic Gold S300). In the next subsection, the parts of the robot are briefly described. Following that, a subsection is presented that describes the time varying moments that were applied to the rigid bodies to drive the model and thus swing the club.

Table 6. Elements and corresponding sections of the shaft.

Element #	Section ID #	Length of Section (in)
1	4	6
2		
3		
4	5	3
5		
6	6	3
7		
8 *	7	1
9 *	8	1
10 *	9	1
11 *	10	1
12 *	11	1
13 *	12	1
14 *	13	1
15 *	14	1
16 *	15	1
17 *	16	1
18 *	17	1
19 *	18	1
20 *	19	1
21 *	20	1
22 *	21	1
23 *	22	1
24 *	23	1
25 *	24	1
26 *	25	1
27 *	26	1
28 *	27	1
29 *	28	1
30 *	29	1
31 *	30	1
32 *	31	1
33 *	32	1
34 *	33	1
35 *	34	1.2
36	35	3.8
37		

* Elements used as variables in the optimization

3.2.2 The Club head

The club head was modeled after the majority of drivers currently in the industry (circa 2004) having a volume of 360 cc. It consisted of eight different parts all of which were meshed using 4-node shell elements. Different parts were used to model the different wall thicknesses of the hollow club head. The wall thicknesses generally vary from around 1 mm on the top of the club, the crown, to 2.3 mm in the face of the club head. All parts, except one, were modeled using the plastic kinematic hardening material in LS-DYNA. This type of material declaration was used to model the high-strength titanium used in most golf club drivers. The final part, which was the hosel where the club head meets the shaft, was modeled as a rigid part. The club head was attached to the shaft in the model by constraining two common nodes and, this material choice was selected solely for joining the club head to the shaft. In the club head to golf ball impact, the hosel does not experience much stress or deformation.

Table 7. Club head components.

PART #	Component of Clubhead	Material	Thickness (mm)
1	Face	Titanium	2.41
2	Crown	Titanium	1.52
3	Sole	Titanium	2.54
4	Backplate	Titanium	1.52
5	Hosel	Steel	2.29
6	Heel	Titanium	1.52
7	Toe	Titanium	1.52
8	Face/Sole Interface	Titanium	2.79

3.2.3 The “Arms”, “Wrists”, and “Hands”

The arms in the swing simulation were represented by a rather section of solid 8-node elements. The elements were all modeled rigidly since in an actual golf robot these elements are made of substantial steel parts. Their true purpose in the model was to

provide a foundation for the applied moments used to initiate and drive the motion of the arms in the mechanical swing of the “Iron Byron”. The block representing the arms is fixed at one end and a moment is applied to the center of mass.

Like the arms, the wrists were rigidly modeled using 8-node solid elements and again their purpose was to provide a foundation for the applied moments in the model. This block of elements was constrained to revolve around a node at the end of the arms. The loading applied to this block of material helped represent the motion of the wrists in the simulation.

The grip was also rigidly modeled and consisted of 4-node shell elements. On the physical Iron Byrons, the grip is a collet mechanism that holds the grip of the club. The shell elements contained in the grip surround the first 10 inches of the shaft in the model. The grip played the role of the hands. It provided a location for the wrist-rolling moment in the golf swing. A load was applied to the grip of the shaft, which allowed the golf club to roll over towards the ball at impact, thus simulating the hands of the mechanical “Iron Byron”.

3.2.4 The Swing: Loading, Joint Definitions, Contact Definitions

The loading in the golf swing consisted of 3 applied time varying moments sufficient to independently drive the arm, wrist release, and wrist roll motions. As hinted at above, one was applied to the rigid part acting as the arm, one to the part acting as the wrists (wrist release), and one to the grip which acted as the hands (wrist roll). In the finite element model, magnitudes of the moments were defined using 3 separate load curves. These load curves had to be carefully iterated and tested to ensure that the swing in the simulation resembled the swing of the mechanical “Iron Byron”. They were also

used to ensure that the club rotated correctly towards the ball making a relatively square impact. The overall club head speed measured at impact in the swing simulation was approximately 120 mph.

The joint definitions in the model also played a role in fine-tuning the swing by allowing for a choice of the wrist release time as happens in the real golf swing. The arms were connected to the wrists by creating a revolute joint in LS-DYNA. Therefore, the part acting as the wrists can revolve around a certain point near the end of the arms. Similarly, the end of the grip was also constrained to revolve around a certain point at the wrists. At the beginning of the simulation the arms, wrists, and grip were all in a locked position and the revolute joints were locked until certain times in the swing. This allows the arms to start the overall downswing. As the block representing the arms rotates due to the applied moment the revolute joint at the wrists unlocks and the club starts revolving around the arms and the wrists. At a final time in the swing, the joint between the wrists and grip unlock and the shaft rotates towards the ball just before impact.

The contact definition between the ball and club head became active in the model when the clubface meets the ball. Both the static and dynamic coefficient of friction values used were 0.3. To save computation time, the ball and club head were switched from deformable to rigid bodies at the beginning of the simulation. Upon ball – club head contact, the club head and ball switch back to deformable for the duration of impact. Once the ball leaves the club head, both were switched. This rigid – deformable switching dramatically cuts down on the computation time required for each simulation of the swing.

3.2.5 The ball

The golf ball in the model consisted of 4 parts, all of which were meshed using 8-node solid elements. The outer layer was modeled as a linear elastic material (moderate stiffness ionomer), while the remaining inner layers were all modeled using the Mooney-Rivlin-rubber material model in LS-DYNA. Essentially, this was a two-piece ball model having single cover and core since the common nodes were merged at time of meshing. The extra parts can be used to model more complex ball designs having cover, mantle, and core(s).

3.3 HEEDS Optimization of Shaft Stiffness

3.3.1 Background / Aim

The optimization strategy presented in this part of the study hopes to establish a method that not only evaluates the performance of various shaft designs but also aims to discover unconventional shaft designs that may have been overlooked.

As shown in Chapter 2, the measure of a golf shaft's "bending profile" or "EI curve" is becoming a benchmark in the golf industry for the evaluation and comparison of golf shaft designs. Some shafts are actually being designed to meet certain "bending profiles". The motivation for the optimization in this part of the study was to find optimum "bending profiles" through evaluating a given full-swing finite element model. The sections that follow explain the implementation of the optimization, its overall objective function, as well as the results.

3.3.2 Baseline Design

In order to prepare the model for the optimization, a traditional shaft design needed to serve as a starting point. This starting point, or baseline design, did not need to satisfy the constraints and objective. However, using a reasonable starting point helped to ensure that the overall swing simulation was consistent and accurate. Details of the problem's constraints and objective will be explained in later sections.

The figures below show the baseline design at different points in the simulation. The different points shown in the figures below are also used to compare the behavior of the optimal designs found in the optimization.



Figure 11. Initial starting point of swing simulation.



Figure 12. Simulation at 0.15 seconds.



Figure 13. Simulation at 0.30 seconds.



Figure 14. Simulation at 0.37 seconds.

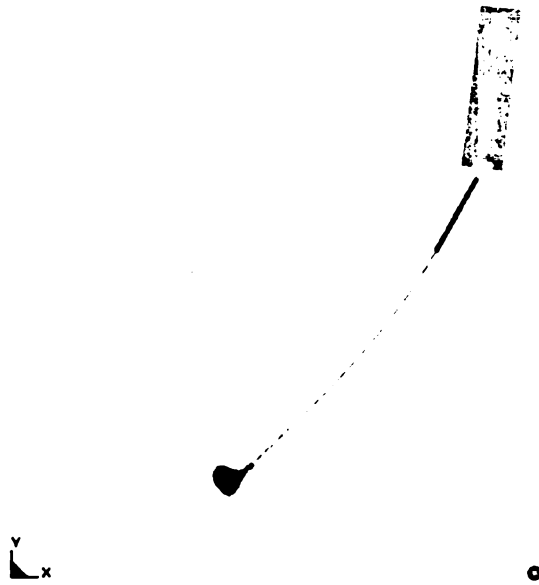


Figure 15. Simulation at 0.41 seconds.

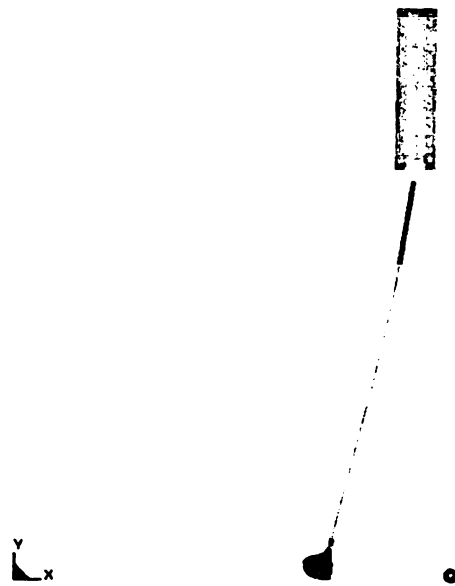


Figure 16. Simulation at 0.42 seconds.

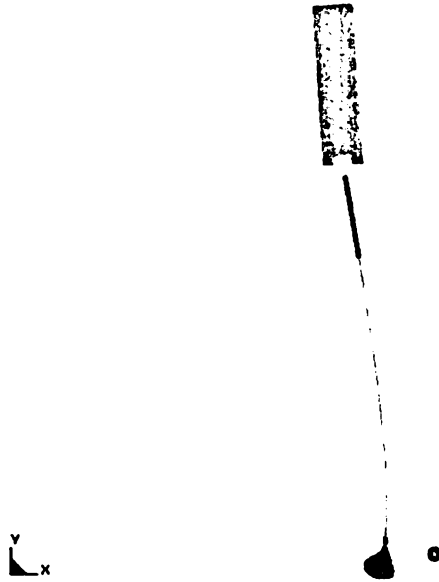


Figure 17. Simulation just after impact at 0.43 seconds.

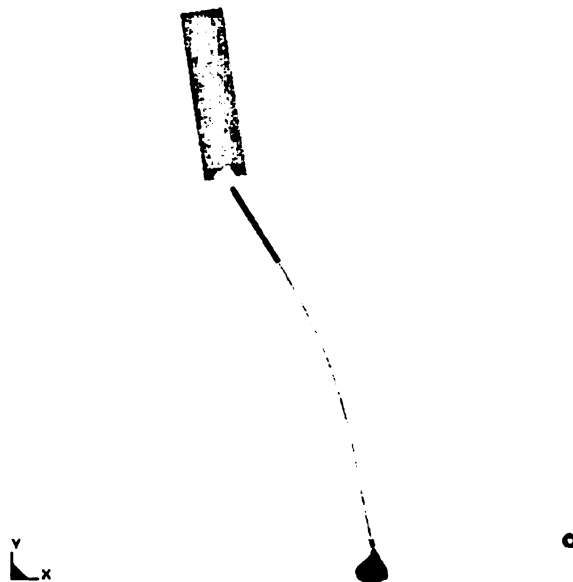


Figure 18. Simulation at 0.44 seconds.

The baseline shaft was modeled after a standard steel golf shaft (True Temper Dynamic Gold S300). The shaft was cut into two inch segments and the radius and thickness were measured. The moment of inertia could then be calculated for each

section of shaft. The figure below shows a breakdown of the stiffness profile used in the baseline design. The range of stiffness in this shaft is typical of most steel and graphite shafts in use today.

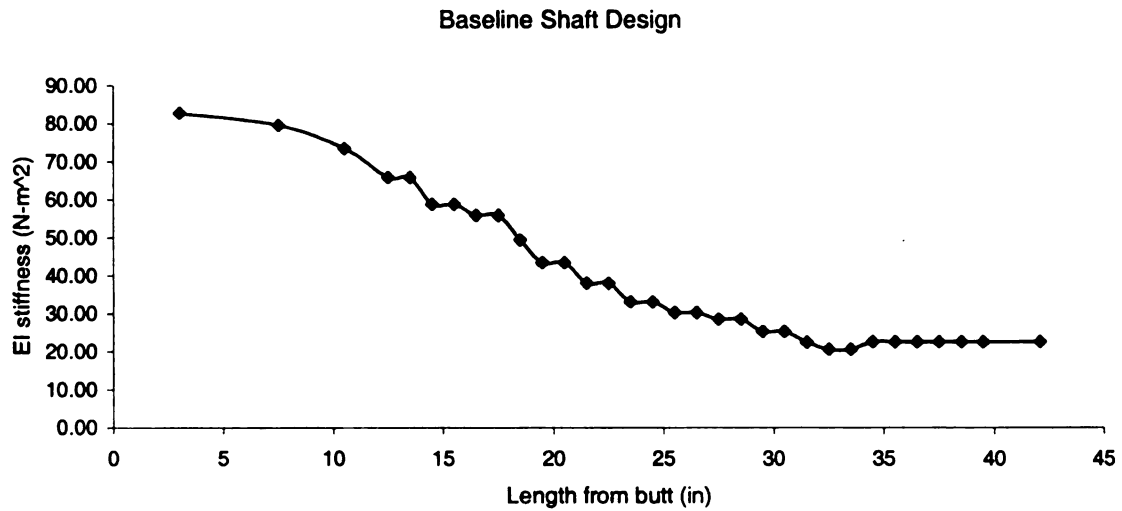


Figure 19. Stiffness profile of baseline shaft design.

3.3.3 Preparations for Optimization

The original model of the swing simulation needed to be modified in various ways to prepare for the optimization and to keep each evaluation as consistent as possible. One of the initial problems involved keeping the impact of the golf ball on the center of the clubface while the stiffness of the shaft was altered from run to run during the optimization. Changes to the stiffness of the shaft would result in minor changes to the location of the club head and location of the resulting impact with the golf ball.

The solution implemented was to separate the LS-DYNA run into two distinct parts. The first part of the simulation was run without the golf ball model. The run was then terminated once a predetermined node on the center of the clubface reached a prescribed location. This location then became the location of impact with the ball. At

this termination point, a small *Perl* script was called that read the position of the predetermined node on the clubface and then translated all nodes of the golf ball accordingly to ensure that the ball made contact with the center of the clubface at impact. This contributed to the consistency of each swing evaluation.

Having moved the ball to ensure it impacted the center of the clubface, the second part of the simulation was run, which included the impact with the golf ball, and the resulting launch and spin characteristics were then evaluated. A diagram detailing the sequence of the simulation is shown below. The next section gives a detailed explanation of the optimization problem.

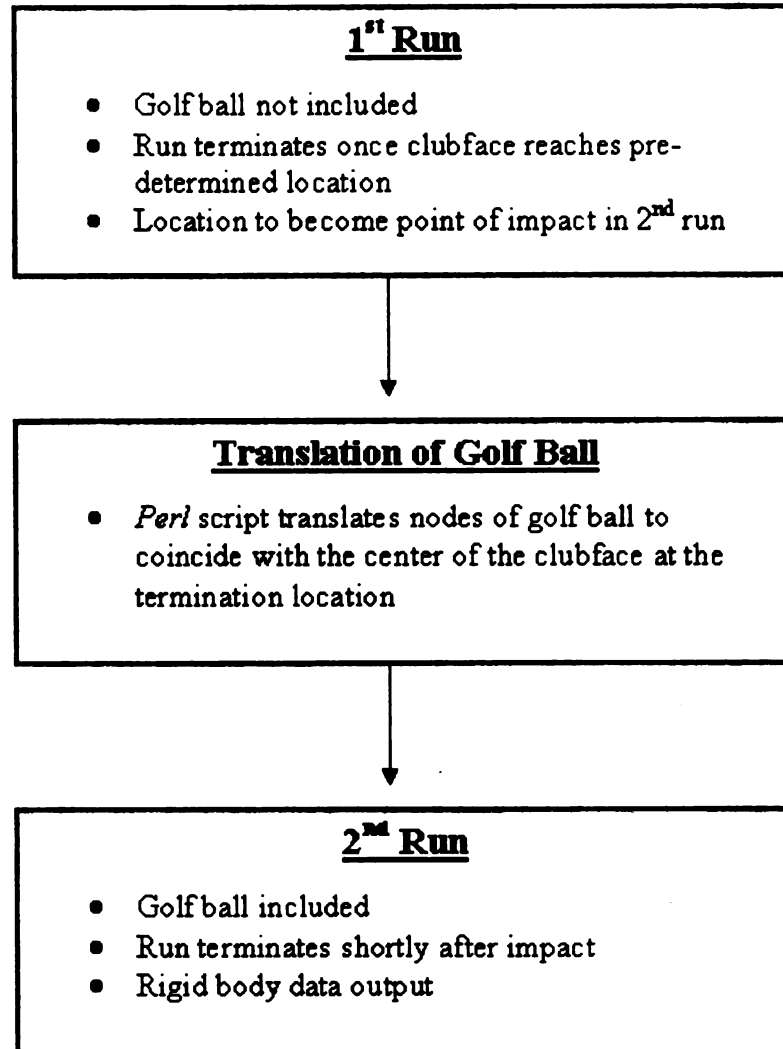


Figure 20. Sequence of swing simulation.

3.3.4 Optimization Problem Definition

To begin defining the optimization problem, the overall objective must first be explained. As the stiffness and geometric properties of the shaft are changed in each run, the resulting trajectory and spin characteristics of the golf ball are examined. The overall objective is to *minimize* the golf ball's backspin, while satisfying other important constraints on trajectory, direction, and velocity magnitude.

As mentioned in a previous section, the swing speed in the simulation was near 120 mph. This swing speed is typical of most low-handicap or professional golfers. At these high swing speeds too much backspin becomes an undesirable characteristic. High backspin causes the golf ball to “balloon” or have too much lift, and can cause considerable losses in driving distance. Therefore the overall objective of the optimization was to find shaft designs that minimize backspin while subject to other constraints on trajectory, direction, and velocity magnitude.

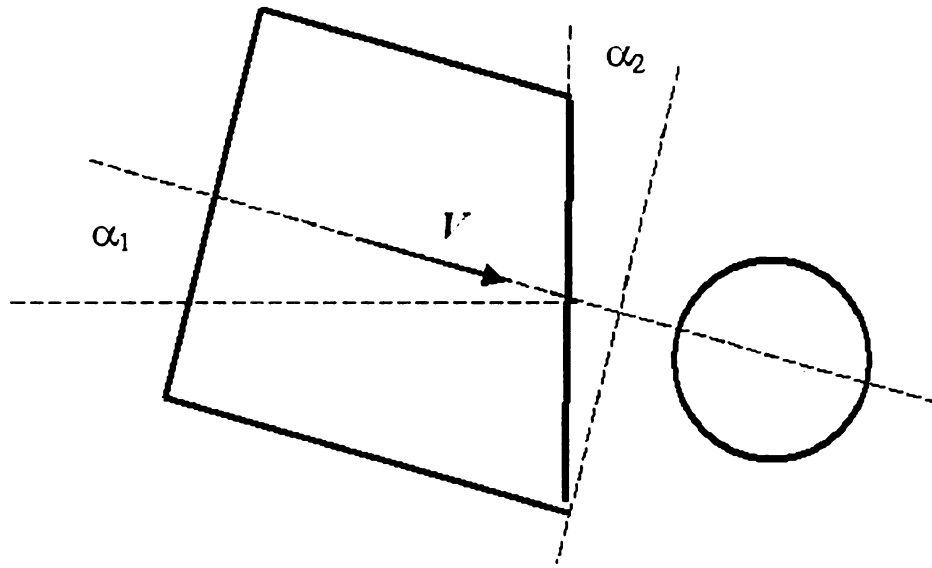


Figure 21. Variables influencing backspin.

The backspin and trajectory characteristics of a golf ball are functions of a limited number of variables in the golf swing. The figure above depicts the three variables that directly influence backspin; the angle of attack α_1 , the clubface loft angle α_2 , and the club head velocity V . These variables are also all functions of the dynamics of the golf shaft during the downswing. In the downswing the shaft is in a bent back position and is “kicked” forward towards the ball at impact. The degree of this action during the

downswing is determined by the bending stiffness properties of the shaft. The goal of the optimization was to investigate the feasibility of unconventional shaft designs that meet the problem objective and that satisfy the basic launch and spin constraints.

3.3.5 Model Variables, Responses, and Constraints

To reiterate, the goal during the optimization is to vary the bending stiffness properties or EI profile of the golf shaft. This was accomplished by keeping the Young's modulus, E , in the material definition constant while varying the moments of inertia I_{xx} and I_{yy} in various elements in the LS-DYNA model. The moments of inertia I_{xx} and I_{yy} are functions of the shafts geometric dimensions, which are the outer radius R_0 and thickness t . These were the primary variables used in the optimization. The assumed outer radius and thickness of each element were varied which in turn varied the moment of inertia and the overall bending stiffness or EI profile of the shaft.

In Section 3.1.1 the details of modeling the shaft in LS-DYNA were discussed and must be noted here. Provided in this section is Table 6, which shows those elements and sections varied during the optimization study. The total length of the shaft was 44 inches. However, portions of the butt and tip ends of the shaft, 12 inches and 3.8 inches respectively, were kept at the standard baseline values. This was a result of the ends of the shaft needing to meet certain dimensions in order to comply with the Rules of Golf and to also allow for the universal assembly of grips and club heads.

The entire mid-section, comprising 28.2 inches, was varied in the optimization study. Over this length the assumed outer radius and thickness for each element were varied. These values were then used to compute the relative entries needed as inputs to the LS-DYNA simulation. They were the moments of inertia I_{xx} and I_{yy} , the polar

moment of inertia J , and the cross-sectional area A . These were all functions of the assumed outer radius and thickness of each element.

An important note to make is in regards to the torsional stiffness (similar to “EI” but termed “GJ”) of the golf shaft. The polar moment of inertia J is indirectly varied during the optimization, which causes the torsional stiffness to vary as well. As stated earlier, the focus of the optimization is on the bending properties of the shaft, however the changes in the torsional stiffness must be addressed and acknowledged. It was assumed that changes in torsional stiffness during the optimization would most dramatically affect the dispersion (directional) angle of the ball flight. Therefore a rather liberal constraint was put on the dispersion angle as will be explained later in this chapter. The torsional stiffness of the shaft was not a major design consideration, however future studies may want to include the modeling of composite golf shafts where this property can be independently studied and optimized.

The difficulty in constraining the outer radius and thickness along the shaft will now be discussed. In each design evaluation, the radii and thickness along the length of the shaft must remain continuous and must also converge upon the butt and tip radii and thickness as well.

The solution found was to use a combination of polynomials to define the radii and thicknesses along the length of the shaft. This would provide continuity and also allow for the values to converge to their tip and butt end values.

In order to implement this in the optimization, a small MATLAB program was created to make these intermediate calculations. The inputs to the program were a series of coordinate points that were used to define the polynomials and therefore the shape and

thickness of the shaft. Once the outer radii and thicknesses of the shaft were defined the program's outputs were then the moments of inertia I_{xx} and I_{yy} , which were then used as inputs to the LS-DYNA swing simulation. The figures and equations below offer a summary of this procedure. Example polynomials are given along with a table showing the allowable range of the coordinate points in the optimization.

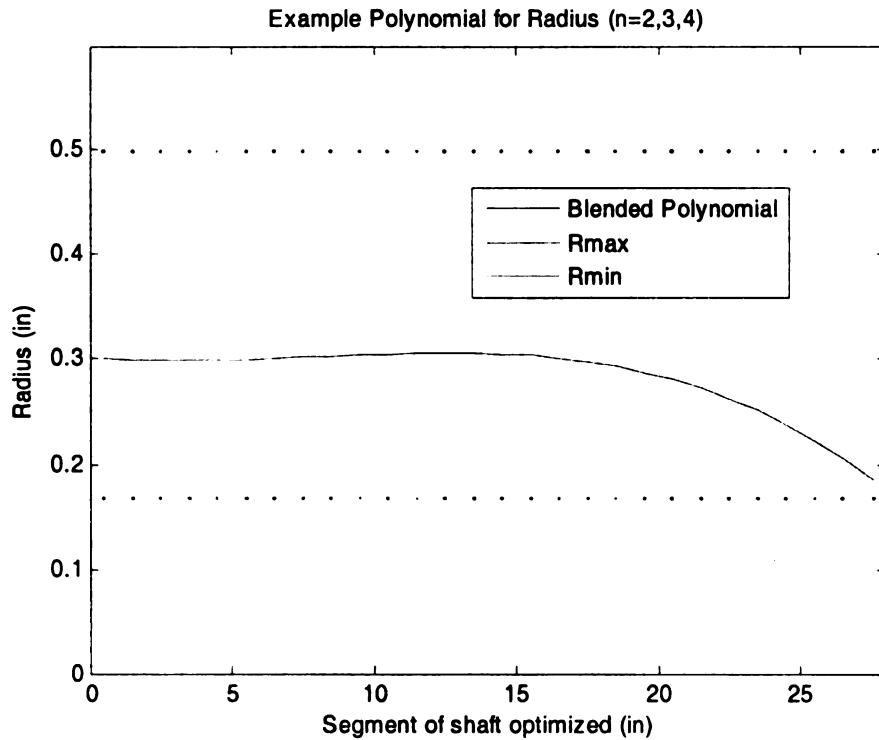


Figure 22. An example polynomial for the outer radius of the shaft. The maximum and minimum allowable radius is also shown.

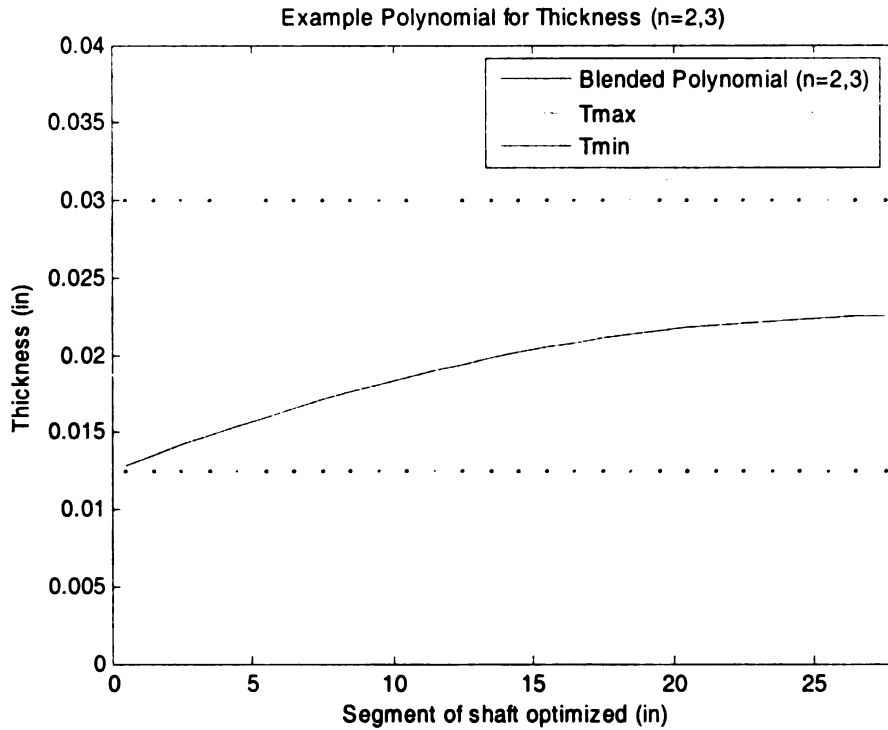


Figure 23. An example polynomial for the thickness of the shaft. The maximum and minimum allowable thickness is also shown.

The radius was defined using a combination of 2nd, 3rd, and 4th order polynomials (n=2,3,4 in title of figure). The coefficients for each respective polynomial were found and then the polynomials were summed and averaged. The generic polynomials below help to explain how this was accomplished.

$$A = ax^2 + bx + c \quad (3.3-1)$$

$$B = fx^3 + gx^2 + hx + j \quad (3.3-2)$$

$$C = kx^4 + mx^3 + nx^2 + px + q \quad (3.3-3)$$

In order to solve for the coefficients of each polynomial, given the two end conditions, each required 1, 2, and 3 coordinate points respectively. The thickness on the other hand used a combination of only 2nd and 3rd order polynomials. Therefore the thickness required 1 and 2 coordinate points for its solution. In all, defining the radius and

thickness along the length of the shaft required a total of 9 x and y coordinate points, therefore 18 overall variables.

A couple of notes must be made regarding the choice of polynomials and the choice of maximum and minimum radius and thickness. The use of higher ordered polynomials was not considered due to the number of variables already being evaluated. More design variables would significantly increase the design space and therefore the number of runs in the optimization. The maximum and minimum constraints on the radius and thickness may also seem conservative but were chosen to meet certain feasibility and manufacturability requirements.

Table 8. Coordinates needed to define polynomials with ranges used in optimization. The X coordinates range over the length of shaft being optimized (0-28.2 in) while the Y coordinates range over the radius and thickness values respectively (all units in inches).

	X1	Y1	X2	Y2	X3	Y3
Radius						
n=2	8 - 20	0.1 - 0.4	--	--	--	--
n=3	6 - 12	0.1 - 0.4	16 - 22	0.1 - 0.4	--	--
n=4	2 - 8	0.1 - 0.4	12 - 16	0.1 - 0.4	20 - 24	0.1 - 0.4
Thickness						
n=2	10 - 18	0.01 - 0.03	--	--	--	--
n=3	6 - 12	0.01 - 0.03	16 - 22	0.01 - 0.03	--	--

The formulas for calculation of the moments of inertia I_{xx} and I_{yy} , polar moment of inertia J , and area A of the shaft are given. The inner radius is simply found from subtracting the thickness from the outer radius.

$$I_{xx} = I_{yy} = \frac{\pi}{4} (R_o^4 - R_i^4) \quad (3.3-4)$$

$$J = \frac{\pi}{2} (R_o^4 - R_i^4) \quad (3.3-5)$$

$$A = \pi(R_o^2 - R_i^2) \quad (3.3-6)$$

The following diagram summarizes the entire sequence of each evaluation in the optimization. This was similar to the previous diagram but also includes the MATLAB implementation.

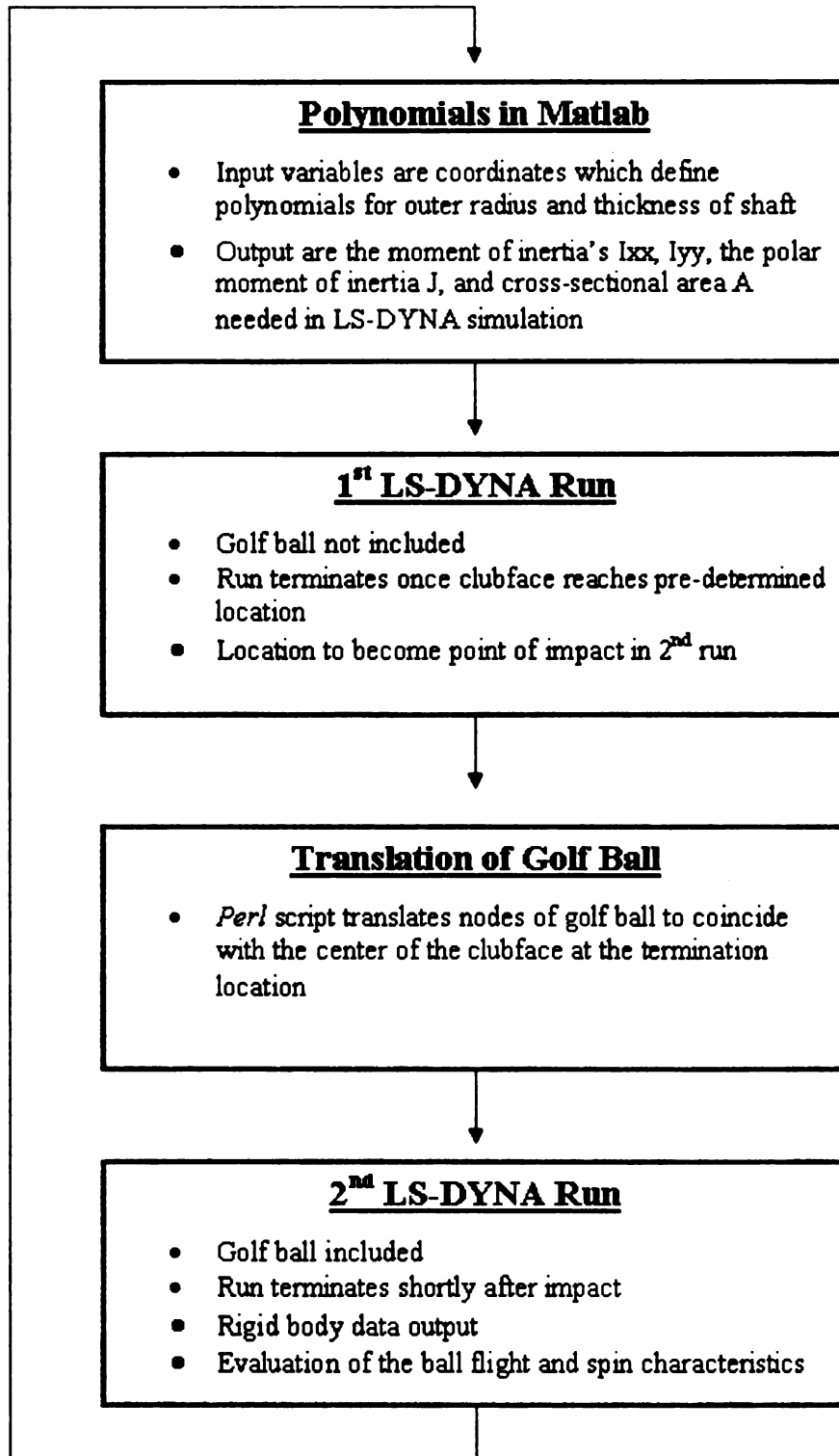


Figure 24. Sequence of one evaluation in optimization.

The constraints and overall objective function of the optimization are now discussed. Each run in the optimization was evaluated by the resulting golf ball flight and spin characteristics after impact. Table 9 is a summary of the various constraints and the objective function.

Table 9. Constraints and objective of optimization.

Response	Type	Target/Norm
X-vel	Prerequisite	
Y-vel	Prerequisite	
Z-vel	Prerequisite	
X-rot	Prerequisite	
Y-rot	Prerequisite	
Z-rot	Prerequisite	
Launch Angle	Constraint	>7 deg, <15 deg
Dispersion Angle	Constraint	<15 deg
Velocity Magnitude	Constraint	>140 mph
Y-rot	Constraint	<200 rad/sec
Backspin	Objective	Minimize

The formulas for calculating the launch and dispersion angles, velocity magnitude, and backspin are given below. The x-axis is the main ball flight direction, the z-axis the off-axis direction, and the y-axis the upward direction.

$$Launch\ Angle = \arctan\left(\frac{Yvel}{Xvel}\right) \quad (3.3-7)$$

$$Dispersion\ Angle = \arctan\left(\frac{Zvel}{Xvel}\right) \quad (3.3-8)$$

$$Velocity\ Magnitude = \sqrt{Xvel^2 + Yvel^2 + Zvel^2} \quad (3.3-9)$$

$$Backspin = Zrot(\cos(DispAng)) - Xrot(\sin(DispAng)) \quad (3.3-10)$$

3.3.6 Results and Evaluation of Optimal Designs

Once the problem was fully developed and defined in HEEDS, the optimization run was executed. 140 different designs were evaluated during the optimization sequence. These designs were then carefully examined.

In the initial stages of evaluating the results, those designs whose performance numbers were similar in magnitude were kept while disregarding the rest. This left a total of 22 shaft designs to be considered. The next step involved plotting their “EI profiles” and eliminating many of the designs that were similar to each other. The “EI profiles” for the most unique designs will now be discussed and compared with the baseline design.

Figure 25 shows the profiles of the first group of optimal designs. The number assigned corresponds to the evaluation number in the optimization. Also shown is the baseline design. As can be seen in Table 10 the overall “best” design found by HEEDS is number 110. Designs that were close in performance but contained slight variations in their profile are also shown in this group of designs.

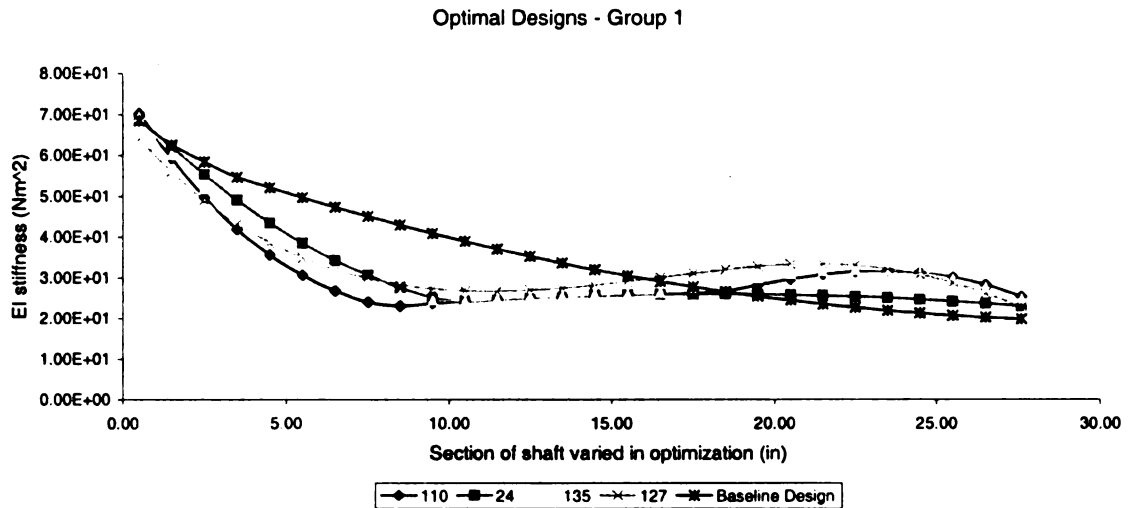


Figure 25. Optimal Designs – Group 1. The profile is that of the 28.2 inch span varied in the optimization.

Figure 26 contains the second group of optimal designs. These designs were separated from the others due to their rather unique EI profiles. They remain relatively close to the “best” design in performance, but have rather unconventional profiles. Two of the designs are similar in that their stiffness declines sharply and then contains a distinctive increase in stiffness near the tip end of the shaft. These are very unique designs but their feasibility must be questioned. The sharp decline in stiffness near the butt end could cause the shaft to snap or break during the downswing.

Optimal Designs - Group 2

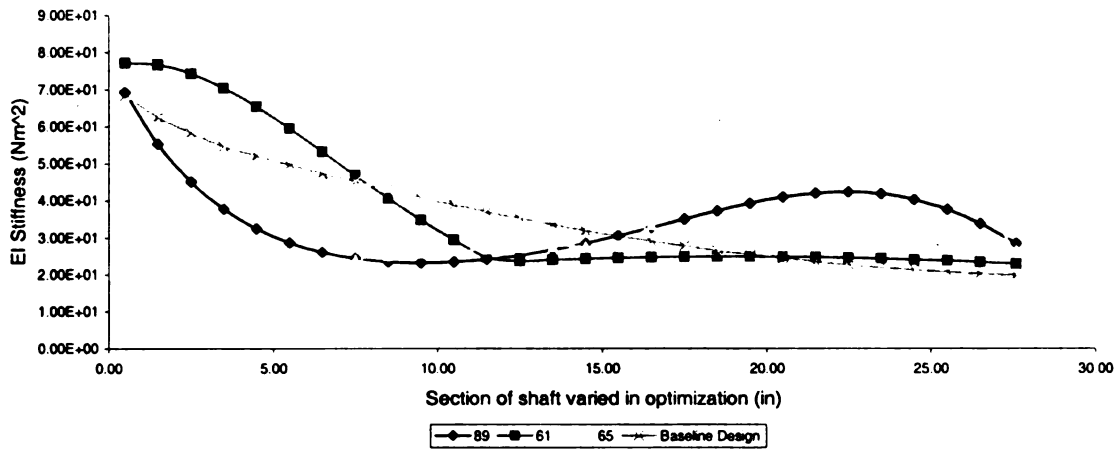


Figure 26. Optimal Designs – Group 2. The profile is that of the 28.2 inch span varied in optimization.

Table 10 gives a summary of the major flight and spin characteristics for both groups of designs. The velocities were all similar in magnitude and the directional angles were well within the constrained limits in the optimization. However a note must be made in regards to the launch angles and backspin rates. Clearly not all of the designs included had necessarily the lowest backspin. This was due to a trade off made when constraining the original optimization problem. The designs with the lowest backspin generally had the lowest launch angles as well. This was somewhat undesirable. A desirable launch angle is around 9-11 degrees, which is well known in the industry as being the optimal launch angle for maximum distance. However it was felt that such a narrow launch angle constraint would over constrain the optimization and therefore overlook design considerations.

Table 10. Ball flight and spin characteristics of optimal designs.

Evaluation #	Performance #	Velocity Magnitude (in/sec)	Directional Angle (deg)	Launch Angle (deg)	Backspin (rpm)
110	0.85	3157	-6.48	7.99	2551
24	0.89	3171	-6.57	8.07	2674
135	0.92	3186	-2.62	8.21	2759
127	1.00	3197	1.28	8.54	2986
89	1.12	3216	-2.73	8.99	3362
61	1.17	3191	2.52	9.43	3516
65	2.63	3105	3.87	7.92	2296

Various designs above were re-run in LS-DYNA in order to compare their swings with the baseline design and to make observations in regards to their feasibility. Each design was chosen carefully.

When compared to the baseline design, no observable differences existed for the first group of optimal designs, therefore making them good design considerations. However the figure below shows design 65 as it was swung. The feasibility of the design must be questioned due to the high degree of deformation occurring in the shaft. No checking of stress levels was done in the current simulations.

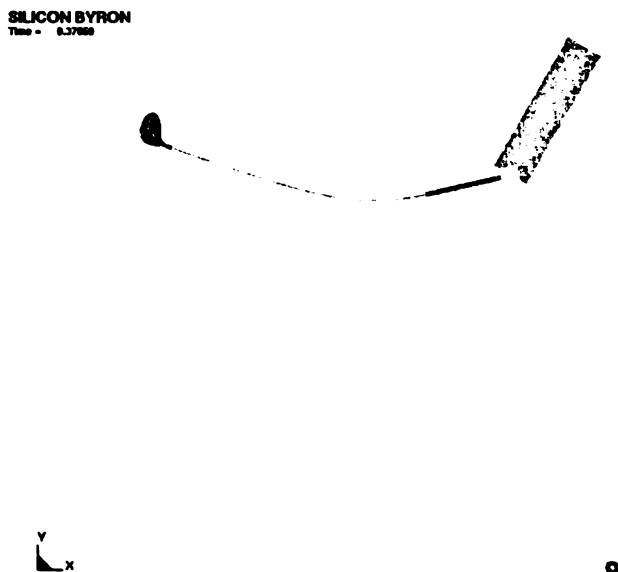


Figure 27. Design 65 exhibiting a high degree of deformation in downswing.

4 Conclusions and Discussion

4.1 Shaft Modeling

A majority of the experimental tests and methods used in the golf industry to help characterize the performance of golf shafts can be modeled and studied analytically. This was accomplished by an initial knowledge of the shaft's "bending profile" or "EI curve". The "zonal frequency" tests as well as the various "kickpoint" tests were modeled using simple beam finite elements.

The calculated zonal frequencies were over-predicted at the higher zones (shorter cantilever lengths) but matched well at the lower zones (longer cantilever lengths). This showed promise in eliminating the need for experimental measurements, but indicated more investigation was needed into modeling the compliance of the frequency measurement device.

The main conclusion drawn from modeling the "kickpoint" tests was that none of these tests or methods lends any real insight into this somewhat elusive property of golf shafts. These tests show no real distinction or relevance in their attempts of measuring this property.

4.2 Optimization

An opportunity was taken to study and optimize the golf shaft using a full swing finite element model with golf ball impact. This allowed for a much broader study of the golf shaft and its influence in the golf swing. The actual dynamics of the golf shaft and its influence on ball flight and spin characteristics were studied and optimized.

The results of the optimization revealed a rather unconventional group of shaft designs as part of the designs considered. Consideration of stress limits on the shaft material should be included in future optimization runs. Prototyping of these designs should be pursued and testing established. As so many know in the golf industry, a new unique shaft design could be marketed very easily.

4.3 Future Work

Based upon the results from the elementary shaft modeling and the successful implementation of the optimization, there are many things to consider for future work.

Modeling of Golf Shafts

- Further investigation of modeling the Fujikura frequency machine and its clamping mechanism
- Researching new dynamic, rather than static, tests for characterization and measurement of “kickpoint”

Optimization

- Prototyping and testing of the optimal shaft designs
- Shaft optimization for a range of swing speeds
- Re-examine loading and joint definitions to model more advanced robots
- Examine experimental data of actual swing kinematics in hopes of modeling an actual subjects golf swing
- Incorporate modeling of graphite composite golf shafts including ply-orientation
- Investigate using prescribed displacements and/or velocities rather than load curves to gain more consistency in evaluating designs in the optimization

Bibliography

- [1] Chou, A., and Roberts, O.C., "Golf Shaft Flex Point – An Analysis of Measurement Techniques", *Science and Golf II: Proceedings of the World Scientific Congress of Golf*, 1994, E&FN Spon, London, pp 278-283
- [2] Mase, T., "Correcting for local circumferential deflections when measuring golf shaft flexural stiffness", *The Engineering of Sport 5 - Conference Proceedings of*, 2004, M. Hubbard and R.D. Mehta and J.M. Pallis, Chicago, pp 515-521
- [3] Horwood G.P., "Golf Shafts – a technical perspective", *Science and Golf II: Proceedings of the World Scientific Congress of Golf*, 1994, E&FN Spon, London, pp 247-258
- [4] Wallace, E.S., and Hubbel, J.E., "The Effect of Golf Club Shaft Stiffness on Golf Performance Variables – Implications for Club-Fitting", *Materials and Science in Sports*, April 2001, pp 23-35
- [5] Butler, J.H., and Winfield, D.C., "The dynamic performance of the golf shaft during the downswing", *Science and Golf II: Proceedings of the World Scientific Congress of Golf*, 1994, E&FN Spon, London, pp 259-264
- [6] Brouillette M., "On Measuring the Flexural Rigidity Distribution of Golf Shafts", *Science and Golf IV: Proceedings of the World Scientific Congress of Golf*, 2002, pp 387-401
- [7] Friedman, Z., and Kosmatka, J. B., "An improved two-node Timoshenko beam finite element", *Computers & Structures*, Volume 47, Issue 3, 1993, pp 473-481
- [8] Lee, M., and Kim, C., "Design optimization of graphite golf shafts based on weight and dynamics of swing", *5th International Conference on the Engineering of Sport (University of California, Davis)*, September 2004, pp 248-255
- [9] Reddy, J.N., *An Introduction to the Finite Element Method*, 2nd Ed., New York: McGraw Hill, 1993
- [10] Przemieniecki, J. S., *Theory of Matrix Structural Analysis*, New York: McGraw Hill, 1968
- [11] Cook R.D., *Concepts and Applications of Finite Element Analysis*, 2nd Ed., New York: Wiley, 1981
- [12] Hughes, T. J.R., *The Finite Element Method: Linear Static and Dynamic Finite Element Analysis*, Englewood Cliffs, N.J.: Prentice-Hall, 1987

- [13] Han, S. M., Benaroya, H., and Wei, T., "Dynamics Of Transversely Vibrating Beams Using Four Engineering Theories", *Journal of Sound and Vibration*, Volume 225, Issue 5, 2 September 1999, pp 935-988
- [14] Winfield, D.C., and Soriano, B.C, "Planar Motion of a Flexible Beam with a Tip Mass Driven by Two Kinematic Rotational Degrees of Freedom", *Journal of Vibrations and Acoustics*, Volume 120, January 1998, pp 206-213

MICHIGAN STATE UNIVERSITY LIBRARIES



3 1293 02736 2601